J. Fluid Mech. (1979), *vol.* 95, *part* 2, *pp.* 305–322
Printed in Great Britain

Propagation of perturbations in the viscous sublayer and adjacent wall region

By HANS-PETER KREPLIN† AND HELMUT ECKELMANN
Max-Planck-Institut für Strömungsforschung
D 3400 Göttingen, West Germany

(Received 13 July 1978 and in revised form 1 May 1979)

The fluctuating velocity components, u and w, and their gradients at the wall,

$$(\partial u/\partial y)|_W \quad \text{and} \quad (\partial w/\partial y)|_W,$$

were measured in a fully developed turbulent channel flow using hot-film probes. The data were taken in an oil channel at a low Reynolds number which allowed velocity measurements very close to the wall. From simultaneous measurements of these signals it could be deduced that coherent flow structures, inclined to the wall, travel downstream. Space-time correlations imply that these are rotating structures. The spanwise distance between these structures was found to be $z^+ \approx 50$ and they could be observed over a streamwise distance of $\Delta x^+ > 1000$.

1. Introduction

Extensive investigations in the last ten to fifteen years in the wall region of bounded turbulent shear flows have shown that the turbulent motion in the vicinity of the wall is not totally random, but partially of a deterministic nature. For more details, reference should be made to the review articles by Willmarth (1975) and Laufer (1975). Visual investigations made by Hama (see Corrsin 1957), Kline *et al.* (1967), Kim, Kline & Reynolds (1971) and more recently by Oldaker & Tiederman (1977) showed that the viscous sublayer of a turbulent boundary layer has a streaky structure. Streaks of high speed fluid alternate with streaks of low speed fluid. Gupta, Laufer & Kaplan (1971) investigated these so-called low speed streaks by means of hot wire anemometry and confirmed the spacing between the low speed streak to be $\lambda^+ \approx 100$ as had been previously found by Kline *et al.* (1967). Corino & Brodkey (1969), Nychas, Hershey & Brodkey (1973) and Offen & Kline (1974) likewise found, by visual investigations, that the fluid motion reveals definite sequences of ordered motions occurring randomly in space and time. Also the velocity patterns obtained by Wallace, Brodkey & Eckelmann (1977) and Eckelmann *et al.* (1977) showed a similar sequence of events. One part of this sequence is the sweep event which was described by Corino & Brodkey (1969) as high speed fluid moving with a velocity usually greater than the mean parallel to or under a slight angle towards the wall. Chen & Blackwelder (1978) used temperature as a passive contaminant and observed sharp internal temperature fronts extending throughout the entire boundary layer. Their velocity data indicated that these

† Present address: DFVLR-AVA Göttingen, D 3400 Göttingen.

0022–1120/79/4340–7840 $02.00

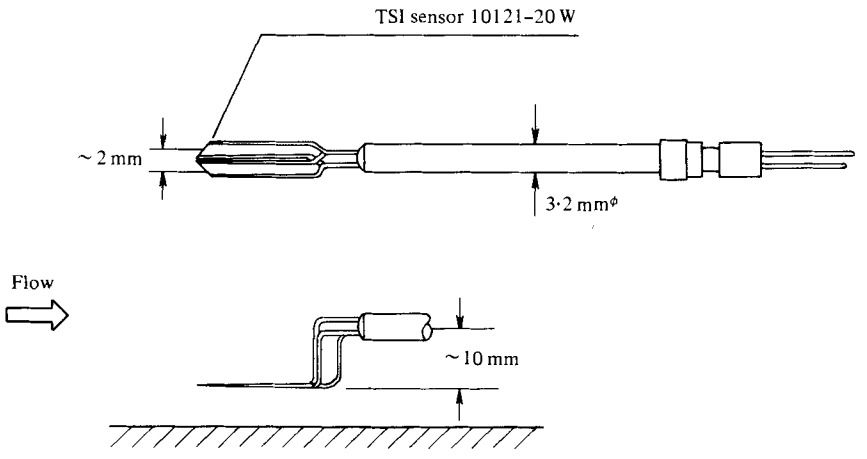

FIGURE 1. Sketch of the V-probe.

fronts were associated with internal shear layers. From space–time correlations in the near wall region in a pipe flow, Bakewell & Lumley (1967) inferred the existence of pairs of counter-rotating streamwise vortices. With electrochemical probes flush mounted in a pipe, Lee, Eckelman & Hanratty (1974) observed a similar pattern. The visual studies of Nychas *et al.* (1973) and Offen & Kline (1974) also showed that there are transverse vortices at intermediate wall distances. In addition Nychas *et al.* (1973) observed the formation of these vortices at the interfaces of advancing high-speed fluid fronts which form an angle with the wall and low-speed fluid regions.

The present work was undertaken using hot-film probe techniques to provide more quantitative data about these fronts in the vicinity of the wall and to find a relation between the fronts and the streaky structure of the wall region.

2. Experimental facility and techniques

The flow facility used for the present investigation was the oil channel at the Max-Planck-Institut für Strömungsforschung originally designed by Reichardt and described by Eckelmann (1970, 1974). Only the unique features of the channel relevant for these investigations are given here. The channel is 8·5 m long, 0·22 m wide and 0·79 m deep and was fully enclosed by a top cover, that was added by Wallace, Eckelmann & Brodkey (1972). The flow was tripped as it entered the channel. The measurements were made 32 channel widths downstream where the flow was fully developed and approximately mid-way between the top cover and the bottom of the channel. The testing fluid was an oil of kinematic viscosity 0·06 cm^2 s^{-1} at 25 °C. For the maximum velocity at the centre-line, $U_{\mathfrak{C}} \approx 21$ cm s^{-1}, the Reynolds-number based on the width of the channel and the centre-line velocity was 7700. For these conditions a distance of 1 cm corresponded to a dimensionless distance of $\lambda^+ = 17$ based on the wall parameters, u_τ and ν.

The co-ordinate system was chosen so that the x axis was aligned with the mean flow direction, y was perpendicular to the wall and z was in spanwise direction. The origin of the co-ordinate system was 32 channel widths downstream of the trip and mid-way between top and bottom of the channel.

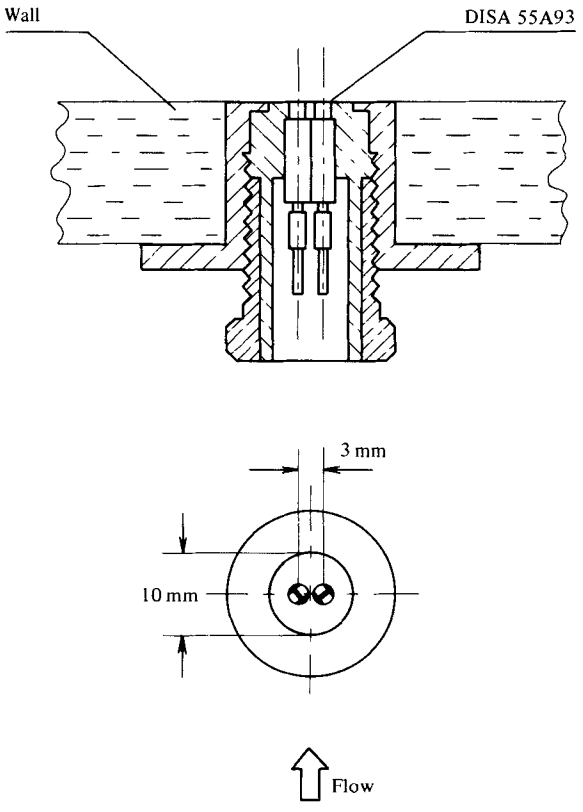

FIGURE 2. Sketch of the wall probe.

The velocity components in x and z direction, $U = \overline{U} + u$ and $W = w$, were measured with quartz coated hot-film probes. Since the flow is two-dimensional, mid-way between the top cover and the bottom, the mean value of the spanwise velocity component, $\overline{W}$, vanishes, so that only a fluctuating component w remains. This component was obtained from the difference signal of two hot-film sensors arranged in a 90° V-configuration to avoid any influence of the instantaneous mean gradient, $\partial U/\partial y$. Such V-probes are not commercially available and were designed by the authors and built using two 1 mm long and 50 μm thick TSI model 10121–20 W sensors. Figure 1 shows a sketch of the V-probe. Because the probe tip is displaced from the probe axis by about 10 mm, it could easily be placed as close to the wall as $y^+ = 1$. A fixed V-probe which was also built using the same type of sensors was mounted on a wall plug at a distance of $y^+ = 2{\cdot}3$.

Heated wall elements were used to measure the two instantaneous velocity gradients at the wall, $(\partial U/\partial y)|_W$ and $(\partial w/\partial y)|_W$. The wall elements are flat hot-films that were flush-mounted in the wall. The sensors, which are quartz coated DISA type 55A93, are 0·75 mm long and 0·15 mm wide. When aligned so that the long axis is perpendicular to the mean flow direction a single sensor was sensitive to the velocity gradient $(\partial U/\partial y)|_W$. For the measurements in this investigation a pair of sensors was used in a V-configuration similar to the V-probe described above. Figure 2 shows a sketch of the wall probe. It was assumed that the sum of the two hot-film wall element signals was

proportional to $(\partial U/\partial y)|_W$ and that the difference was proportional to $(\partial w/\partial y)|_W$. Making the same assumptions Sirkar & Hanratty (1970) used similar V-configurations of electro-chemical sensors to measure these two velocity gradients at the wall. The wall elements and hot-film probes were driven by TSI Model 1050 anemometers. The signals of the wall elements were linearized by DISA 55D10 linearizers and the signals of the V-probe by TSI Model 1052 linearizers. The operation resistance of the wall elements R_w was chosen to be 2% and that of the V-probe 1% higher than the resistances at room temperature R_c which yielded an overheat ratio $R_w/R_c = 1{\cdot}02$ for the wall elements and $R_w/R_c = 1{\cdot}01$ for the V-probes. These low overheat ratios were possible since the temperature of the entire laboratory including the oil channel was controlled. The frequency response for all probes used was measured by the square-wave method and was found to be the same as earlier determined by Eckelmann (1974). For both the earlier measurements and for the present investigation, the flow channel used was the same and the sensors of the probes were similar. Errors due to convection at low velocities, temperature fluctuations and the influence of high turbulence intensities have also been discussed by Eckelmann (1974). A sufficient number of V-wall elements was available so that many spatial separations in the x or z direction could be obtained. Since the wall elements were mounted flush in the wall and the overheat temperature was very low (8 °C), they did not cause any physical probe interference.

The calibration of the movable V-probe was accomplished by towing it with variable speeds through the oil at rest. The wall elements and the fixed V-probe were calibrated by running the channel at three different speeds corresponding to known mean velocity gradients at the wall. These had been previously determined by transversing a single hot-film probe through the viscous sublayer. The range of the linear velocity profile in the oil channel is $y \lesssim 3$ mm. It is thus easy to place a single probe within this layer at several positions to determine the velocity gradient at the wall. At this relatively large wall distance, no wall effects were observed. The streamwise velocity gradient $(\partial U/\partial y)|_W$ from the V-wall elements was obtained from the sum of the linearized signals and the spanwise velocity gradient $(\partial w/\partial y)|_W$ from the difference. The same technique was used for both V-probes. Since in a fully developed turbulent channel flow $\overline{W}$ and $(\partial \overline{W}/\partial y)|_W$ are zero, the mean values of the difference signals were adjusted to zero. Any remaining systematic error was checked by calculating the correlation coefficients between the streamwise and spanwise components, which should be zero by homogeneity, and by calculating the skewness factors of the spanwise components, which should be zero from symmetry considerations. It was typically found that

$$\frac{\overline{uw}}{u'w'}, \quad \frac{\overline{(\partial u/\partial y)|_W\,(\partial w/\partial y)|_W}}{(\partial u/\partial y)|'_W\,(\partial w/\partial y)|'_W} \quad \text{and} \quad \frac{\overline{w^3}}{(w')^3}, \quad \frac{\overline{((\partial w/\partial y)|_W)^3}}{((\partial w/\partial y)|'_W)^3}$$

were of the order of $\pm$ 0·05. The primes in the denominators denote r.m.s. values.

The calibration of the probes was done in the laboratory using analog techniques, whereas digital techniques were used for the measurements. Since only a 10 bit analog-to-digital converter was available a constant d.c. voltage was subtracted from each of the signals which was approximately equal to the d.c. component of the signals. The signals were then amplified and sent over analog lines to a PDP-15 computer where they were digitized (sample and hold) at a rate of 50 samples per second for 20 to 30

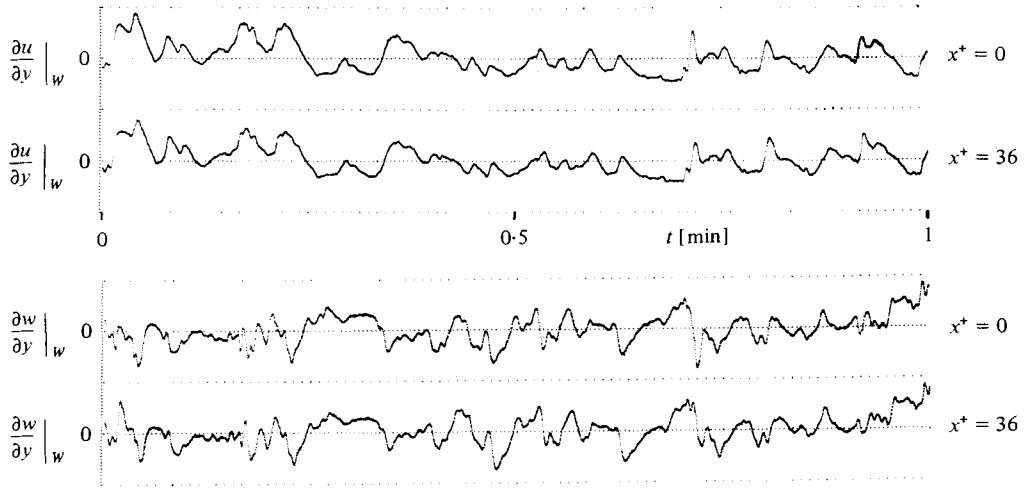

FIGURE 3. Simultaneous records of the fluctuating wall gradients with $\Delta x^+ = 36$, $\Delta z^+ = 0$.

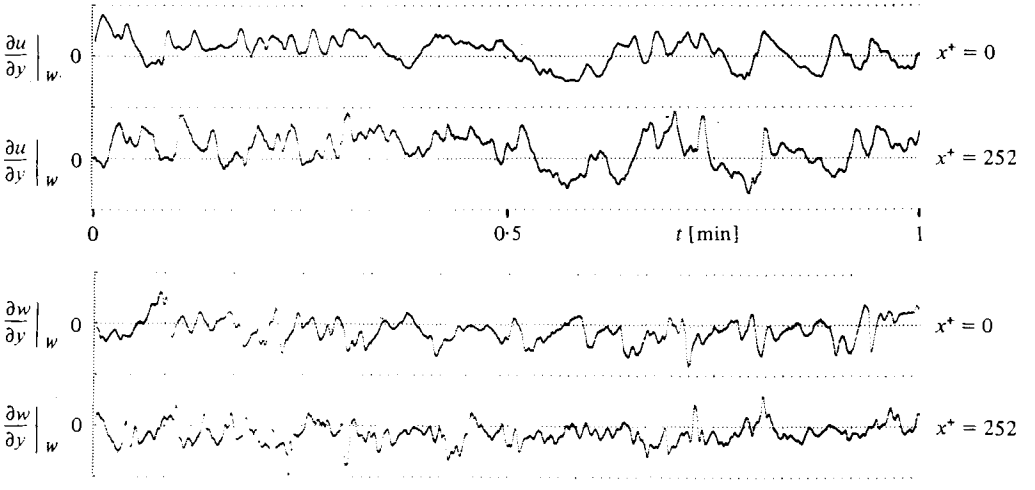

FIGURE 4. Simultaneous records of the fluctuating wall gradients with $\Delta x^+ = 252$, $\Delta z^+ = 0$.

minutes and stored on a magnetic disk. These run times were sufficient to obtain adequate statistical samples. The analysis of the stored data was done by assembler and FORTRAN programs. More details are given in the dissertation of Kreplin (1976).

3. Space–time correlations of the velocity gradient at the wall

The correlations of the fluctuations of the velocity gradients at the wall $(\partial u/\partial y)|_W$ and $(\partial w/\partial y)|_W$ were obtained from two pairs of wall elements at various positions. For each measurement, only one co-ordinate was varied, either the x or the z co-ordinate. Usually the measurement of correlations with streamwise separations are difficult because the downstream probe lies in the wake of the upstream probe. In this work, the disturbing wakes were avoided by using the flush-mounted wall elements. The

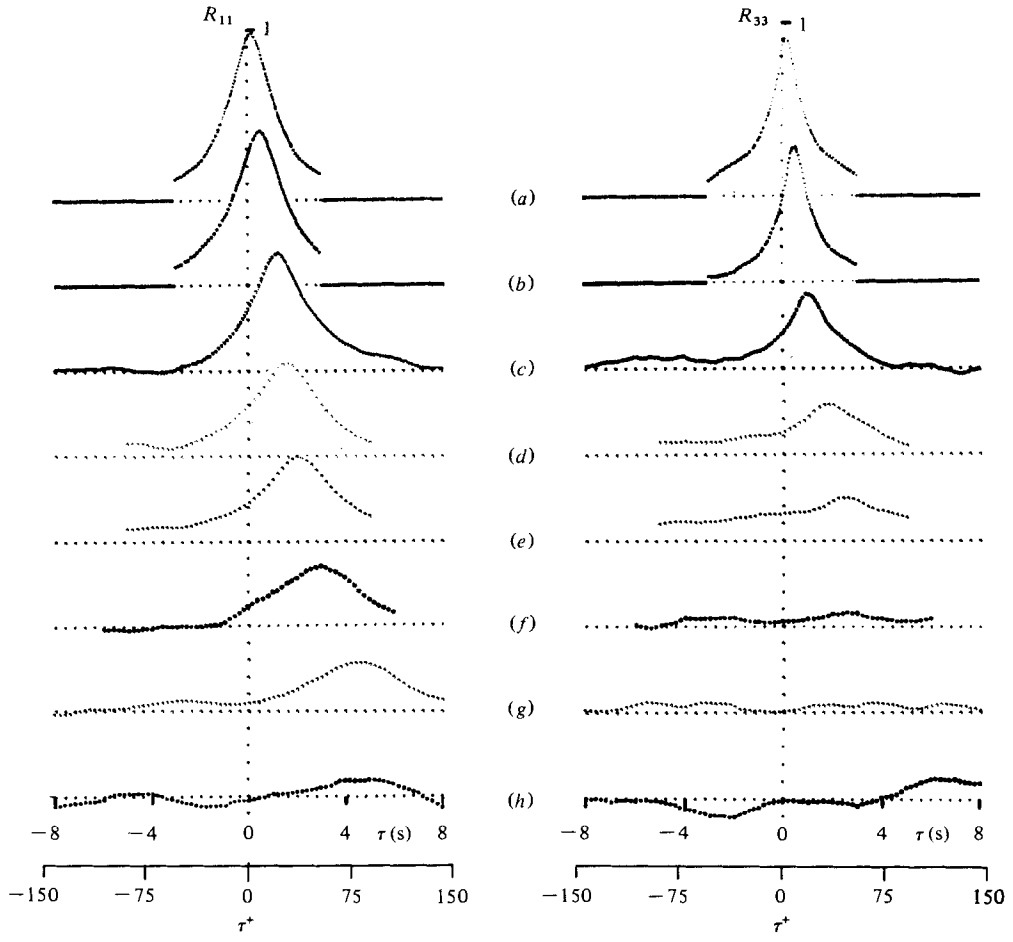

FIGURE 5. Streamwise space–time correlations of $(\partial u/\partial y)|_W$ and $(\partial w/\partial y)|_W$ as a function of Δx^+. $(\Delta x^+, x/b)$: (*a*), (36, 0·18); (*b*), (108, 0·54); (*c*), (252, 1·3); (*d*), (378, 1·9); (*e*), (486, 2·4); (*f*), (792, 4·0); (*g*), (1044, 5·2); (*h*), (1280, 6·4).

low overheat temperature of 8 °C was sufficient to cause no measurable thermal wake effects.

3.1. *Streamwise space–time correlations*

The time functions of the fluctuations $(\partial u/\partial y)|_W$ and $(\partial w/\partial y)|_W$ obtained from two pairs of wall elements are plotted in figures 3 and 4 for probe separations $\Delta x^+ = 36$, $\Delta z^+ = 0$ and $\Delta x^+ = 252$, $\Delta z^+ = 0$. At the smaller probe separation (figure 3) the signals of both the streamwise and the spanwise fluctuations are very similar and there is a small time shift between the signals with the upstream probe signals leading the signals obtained from the downstream probe. With increasing probe separation the time shift increases and the similarity of the signals decreases (figure 4).

In order to determine the average time shift, the normalized correlation functions

$$R_{11}(\Delta x, \tau) = \frac{\overline{[\partial u(x,t)/\partial y]|_W . [\partial u(x+\Delta x, t+\tau)/\partial y]|_W}}{[\partial u(x)/\partial y]|'_W . [\partial u(x+\Delta x)/\partial y]|'_W}$$

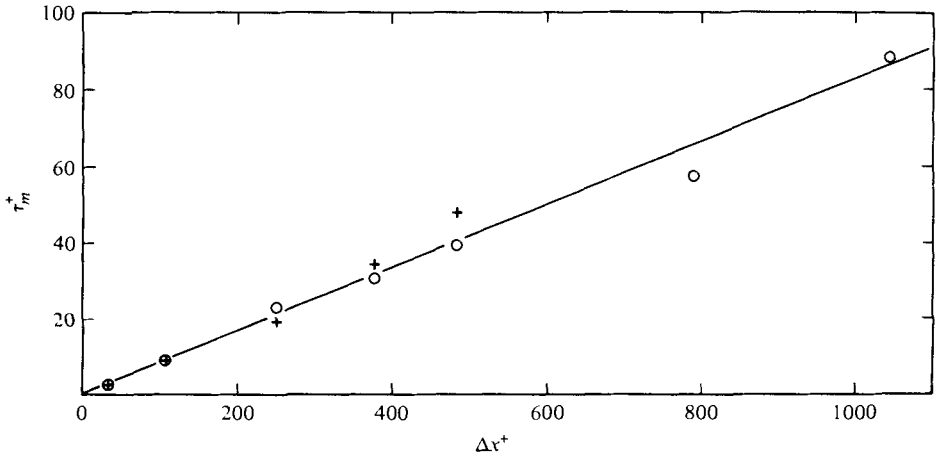

FIGURE 6. Time shifts for maximum correlation as a function of the distance Δx^+. ○, R_{11}; +, R_{33}.

and
$$R_{33}(\Delta x, \tau) = \frac{\overline{[\partial w(x,t)/\partial y]|_W . [\partial w(x+\Delta x, t+\tau)/\partial y]|_W}}{[\partial w(x)/\partial y]|'_W . [\partial w(x+\Delta x)/\partial y]|'_W}$$

were calculated. The result is shown in figure 5 for various separations in the streamwise direction. The zero-lines of the correlation curves are displaced by 0·5 in the ordinate. The time axis is the same for all curves ($\tau = \pm 8$ s corresponding to

$$\tau^+ = \tau u_\tau^2/\nu \approx \pm 150).$$

As has already been seen from the time functions of figures 3 and 4, both the streamwise and spanwise fluctuations are highly correlated with the correlation decreasing as the separation distance increases. The streamwise fluctuations are correlated for larger distances than the spanwise fluctuations. At a distance of $\Delta x^+ = 1044$, which corresponds to about five times the channel half-width, b, the maximum correlation of the streamwise fluctuations still reaches a value of 0·3. Space–time correlation measurements in the same oil channel by Blackwelder & Eckelmann (1978) led to a similar result.

As Δx^+ increases, the maxima of the correlation curves shift towards larger times, τ. In figure 6 the non-dimensional time shifts, τ_m^+, obtained from the locations of the maxima of the correlation functions of figure 5 are plotted *versus* the non-dimensional separation distances Δx^+. τ_m^+ increases linearly with Δx^+ within the range of scatter. This means that there exits a constant convection velocity of $c_x = \Delta x^+/\tau_m^+ = 12{\cdot}1 u_\tau$ for both, the streamwise and spanwise fluctuations at the wall. This value corresponds to the local mean velocity at a distance from the wall of $y^+ = 17$, which is approximately the same distance where the maximum turbulence production occurs. Compared to the centre-line velocity, the convection velocity is $c_x = 0{\cdot}62 U_{\mathfrak{C}}$.

The streamwise space–time correlation measurements of the wall pressure fluctuations in a turbulent boundary layer by Willmarth & Wooldridge (1962), Bull (1967) and Blake (1970) show a nonlinear relationship between the separation distance of the pressure probes, Δx, and the time shifts of the maxima of the correlation curves, τ_m. For the convection velocity of the pressure fluctuations, defined as $c_c = d\Delta x/d\tau_m$,

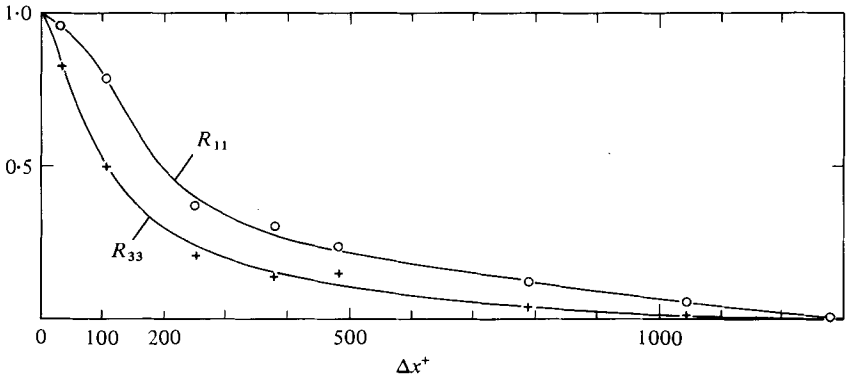

FIGURE 7. Streamwise correlations at $\tau^+ = 0$ and $\Delta z^+ = 0$ of $(\partial u/\partial y)|_W$ and $(\partial w/\partial y)|_W$ as a function of Δx^+.

values of $c_c/U_\infty = 0{\cdot}53$ to $0{\cdot}83$ were obtained, where U_∞ is the free stream velocity. The convection velocity of the pressure fluctuations moving downstream increases with the separation distance between the pressure probes. The value $c_c/U_\infty = 0{\cdot}83$ is valid for the separations $10 \lesssim \Delta x/\delta^* \lesssim 20$ and $c_c/U_\infty = 0{\cdot}53$ is obtained for $\Delta x \to 0$. This dependence of the convection velocity on the probe separation was explained by Willmarth & Wooldridge (1962) as follows. It was assumed that the sources of the wall pressure fluctuations are structures that move downstream in the flow. For small probe separations, the correlation is determined primarily by the smaller structures in the wall region which travel downstream at slower velocities. With larger probe separations, the small structures decay significantly as they travel between the pressure transducers and the faster moving, larger structures dominate the correlations and hence yield a higher convection velocity. The convection velocity of the fluctuations of the velocity gradient at the wall of $c_x/U_\infty = 0{\cdot}62$, obtained in the present investigation lies well within the range of the convection velocity of wall pressure fluctuations; but this velocity is independent of the separation distance between the wall elements.

Emmerling (1973) and Emmerling, Meier & Dinkelacker (1974) used an optical method to investigate the instantaneous structure of the wall pressure beneath a turbulent boundary layer. They found that local extrema of the wall pressure move in the mean flow direction with instantaneous convection velocities of $c_c/U_\infty = 0{\cdot}39$ to $0{\cdot}82$; with values of $0{\cdot}53$ to $0{\cdot}73$ being most probable. The wall pressure extrema gradually changed their form as they travel downstream and they could be followed over the whole field of view of $\Delta x^+ \approx 900$. The mean value of the wall pressure convection velocity is in good agreement with the mean propagation velocity of the fluctuations of the velocity gradient at the wall.

The streamwise spatial correlations from figure 5 with $\tau = 0$ of the streamwise and spanwise fluctuations of the velocity gradient at the wall ($R_{11}(\Delta x^+)$, $R_{33}(\Delta x^+)$) are shown in figure 7 as they vary with the nondimensional probe distance Δx^+. The maximum length over which correlation exists agrees well with the value of Emmerling (1973). The length of a low speed streak, which can easily be estimated from the film of Oldaker & Tiederman (1977), also falls into this range. One must imagine that the length of $\Delta x^+ \approx 1200$ obtained from $R_{11}(\Delta x^+)$ is a minimum extent of those streaks because they meander or move under a slight angle downstream, which considerably

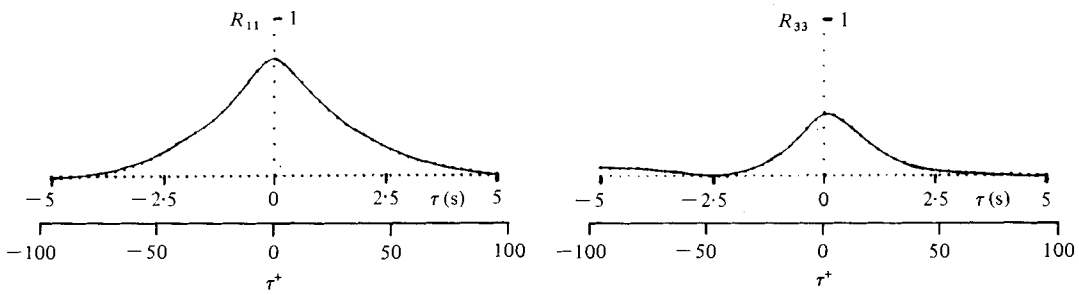

FIGURE 8. Spanwise space–time correlations of $(\partial u/\partial y)|_W$ and $(\partial w/\partial y)|_W$ for $\Delta x^+ = 0$ and $\Delta z^+ = 12{\cdot}6$.

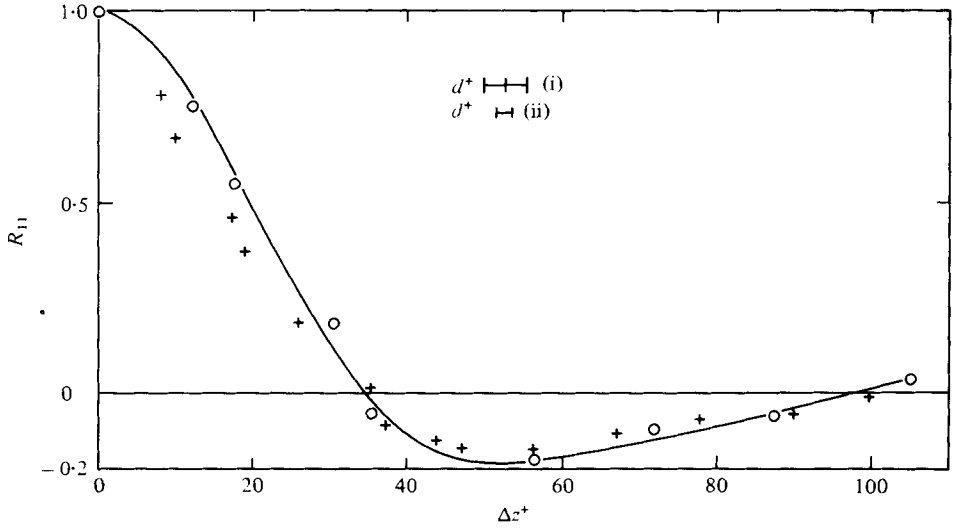

FIGURE 9. Spanwise correlation at $\tau^+ = 0$ and $\Delta x^+ = 0$ of $(\partial u/\partial y)|_W$ as a function of Δz^+, $Re = 7700$. (i) Present investigation: ○; (ii) Simpson's (1976) results: +.

reduces the length scales of the correlation. The correlation $R_{33}(\Delta x^+)$ will be discussed in a later paragraph.

From the results presented in this section it can be concluded that streamwise elongated structures exist in the turbulent flow field which move with an average convection velocity of about 60% of the centre-line velocity. The 'footprints' of these structures can be followed in the flow channel over a distance of six channel half widths.

3.2. *Spanwise space–time correlations*

The spanwise space–time correlations of the fluctuations of the velocity gradient at the wall, $(\partial u/\partial y)|_W$ and $(\partial w/\partial y)|_W$, were measured with two pairs of wall elements, which had the same x but different z co-ordinates ($12{\cdot}6 \leqslant \Delta z^+ \leqslant 105$). The correlations

$$R_{11}(\Delta z, \tau) = \frac{\overline{[\partial u(z,t)/\partial y]|_W . [\partial u(z+\Delta z, t+\tau)/\partial y]|_W}}{[\partial u(z)/\partial y]|'_W . [\partial u(z+\Delta z)/\partial y]|'_W}$$

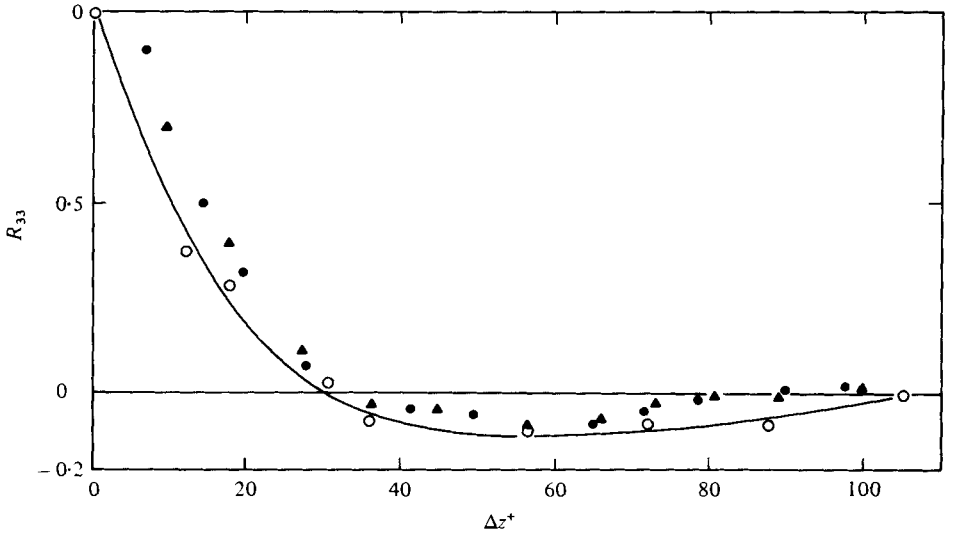

FIGURE 10. Spanwise correlation at $\tau^+ = 0$ and $\Delta x^+ = 0$ of $(\partial w/\partial y)|_W$ as a function of Δz^+. ○, present investigation, $Re = 7700$; ●, Lee *et al.* (1974), $Re = 26900$; ▲, Lee *et al.* (1974), $Re = 35900$.

and

$$R_{33}(\Delta z, \tau) = \frac{\overline{[\partial w(z,t)/\partial y]|_W . [\partial w(z+\Delta z, t+\tau)/\partial y]|_W}}{[\partial w(z)/\partial y]|'_W . [\partial w(z+\Delta z)/\partial y]|'_W}$$

for the distance $\Delta z^+ = 12{\cdot}6$ are shown as an example in figure 8. These curves have their maximum at the time $\tau = 0$ and are symmetric, as are the correlation curves at the other distances Δz^+, which are not shown here.

The spanwise spatial correlation functions $R_{11}(\Delta z^+)$, $R_{33}(\Delta z^+)$ of $(\partial u/\partial y)|_W$ and $(\partial w/\partial y)|_W$ as they vary with the non-dimensional probe distance Δz^+ are shown in figures 9 and 10. The plotted points are the values of the space–time correlations for zero time shift. Both correlations decrease rapidly with increasing distance and become negative at $\Delta z^+ \approx 30$. There is also a broad minimum in both cases at $\Delta z^+ \approx 50$. The correlation is nearly zero at distances $\Delta z^+ > 100$. An additional maximum at greater Δz^+ could not be observed. For purposes of comparison, results obtained by Simpson (1976) in the same oil channel flow but using flush-mounted hot-film elements he designed and constructed are also shown in figure 9. The results agree well with those of the present investigation except for a systematic deviation at small distances Δz^+, which can be explained by the different dimensions of the probes. The width of our wall elements, $d^+ = 5{\cdot}4$, which consist of two hot-film probes, was about three times that of Simpson's single element. For comparison the dimensions of the probes are also shown in figure 9.

In a turbulent pipe flow at Reynolds numbers 26900 and 35900 the spanwise correlation $R_{33}(\Delta z^+)$ has also been measured by Lee, Eckelman & Hanratty (1974) using an electro-chemical method. A comparison with their results is made in figure 10. The agreement with the present investigation is reasonable.

The correlation

$$R_{13}(\Delta z, \tau) = \frac{\overline{[\partial u(z,t)/\partial y]|_W . [\partial w(z+\Delta z, t+\tau)/\partial y]|_W}}{[\partial u(z)/\partial y]|'_W . [\partial w(z+\Delta z)/\partial y]|'_W}$$

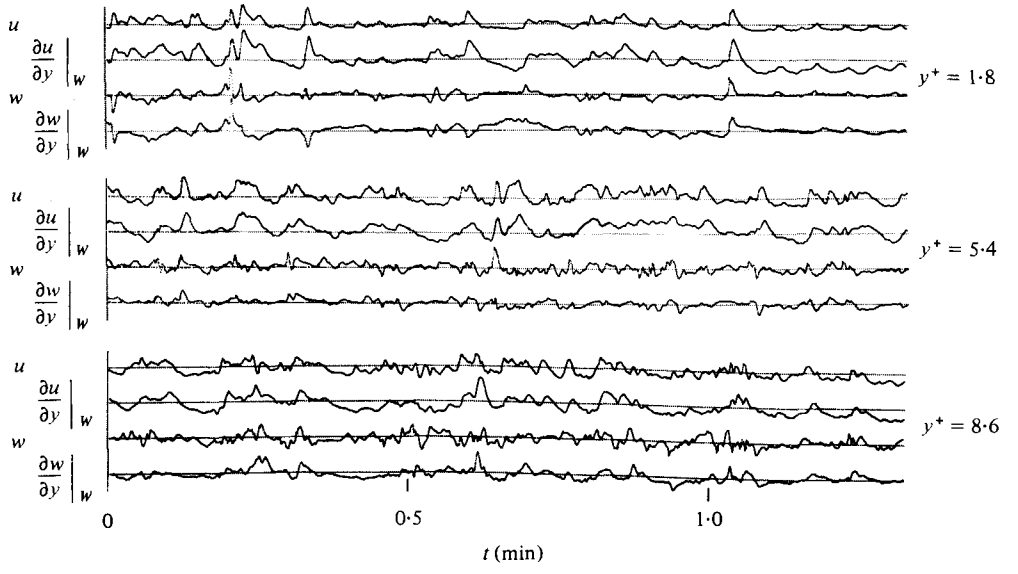

FIGURE 11. Simultaneous records of velocities and wall gradients with $\Delta x^+ = \Delta z^+ = 0$.

has not been measured by the present authors, but was reported by Blackwelder & Eckelmann (1978) from measurements made in the oil channel using the same wall elements.

From these spanwise space–time correlations it is concluded that the structures observed at the wall are as narrow as $\Delta z^+ \approx 50$. This is one half the distance of the low speed separation reported by Kline *et al.* (1967) and Gupta *et al.* (1971).

4. Space–time correlations of the streamwise and spanwise fluctuations of the velocity and the velocity gradient at the wall

The streamwise and spanwise fluctuations of both the velocity and the velocity gradient at the wall were simultaneously measured with a V-probe at various wall distances, y, and with a wall probe consisting of a pair of wall elements. Here the x and z co-ordinates of both probes were the same. In figure 11 time functions of these fluctuations are plotted for three different wall distances. The streamwise fluctuations show the similarity and the increasing time shift with the wall distance described by Eckelmann (1970, 1974). The spanwise fluctuations are also very similar, but this similarity decreases much more rapidly with the wall distance than that of the streamwise fluctuations. The time shift between the spanwise fluctuations also increases with increasing wall distance. In order to determine this time shift, the correlations

$$R_{11}(y,\tau) = \frac{\overline{u(y,t).[\partial u(0,t+\tau)/\partial y]}}{u'(y).(\partial u(0)/\partial y)'}$$

and

$$R_{33}(y,\tau) = \frac{\overline{w(y,t).[\partial w(0,t+\tau)/\partial y]}}{w'(y).(\partial w(0)/\partial y)'}$$

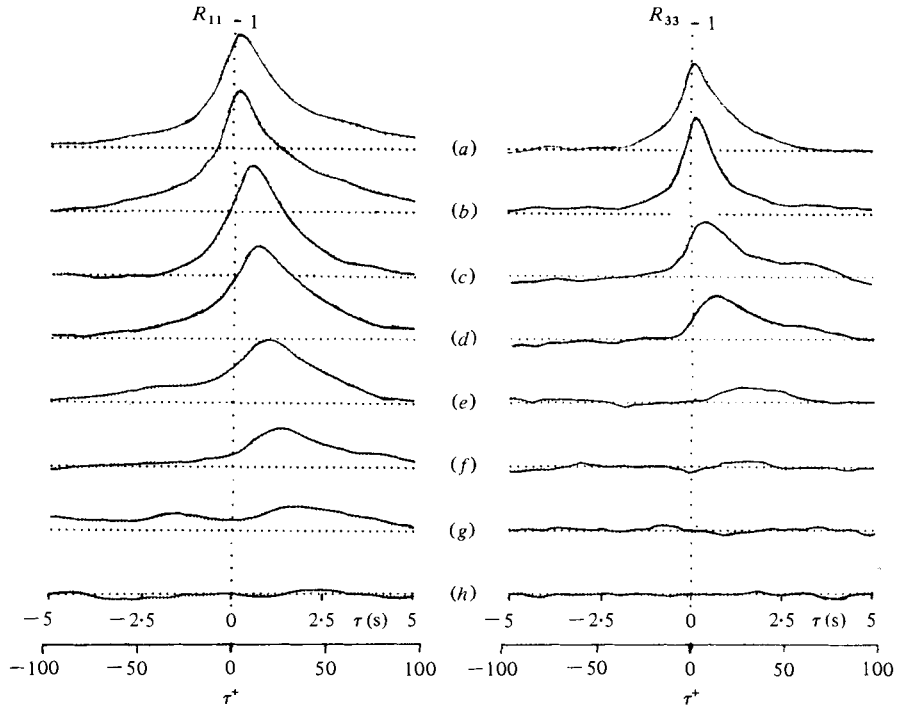

FIGURE 12. Space–time correlations between u and $(\partial u/\partial y)|_w$ (left) and between w and $(\partial w/\partial y)|_w$ (right) as a function of y^+ for $\Delta x^+ = \Delta z^+ = 0$. $(y^+, y/b)$: (*a*), (1·8, 0·01); (*b*), (3·6, 0·02); (*c*), (8·6, 0·04); (*d*), (16, 0·08); (*e*), (31, 0·16); (*f*), (50, 0·25); (*g*), (100, 0·5); (*h*), (200, 1·0).

were calculated and plotted in figure 12. As in figure 5 the zero-lines of the correlation curves are displaced by 0·5 in the ordinate. The time axis is the same for all curves ($\tau = \pm 5$ s corresponding to $\tau^+ \approx 100$). As indicated by the time functions of figure 11, the streamwise fluctuations are highly correlated at small distances. The correlations of the spanwise fluctuations behave similarly to those of the streamwise fluctuations; however, the correlation is less pronounced and a distinct maximum can no longer be discerned for wall distances $y^+ > 31$. On the other hand, the streamwise fluctuations show a positive correlation for all wall distances except at the channel centre-line ($y^+ = 200$). The maximum of the correlation curves of the streamwise and spanwise fluctuations is shifted to greater times τ as the wall distance increases with the signals at the V-probe leading those of the wall element. Thus, it is seen that perturbations in the streamwise and spanwise velocity component propagate toward the wall.

In figure 13 the non-dimensional time shifts, τ_m^+, of the maxima of the correlation functions of figure 10 are plotted versus the non-dimensional wall distance y^+. Values obtained by Eckelmann (1970, 1974) are also given in figure 13. τ_m^+ is found to be proportional to the wall distance in the viscous sublayer ($y^+ \lesssim 5$). If the perturbations are considered to have a propagation velocity c_y, it can be determined by using the wall distance y and the time shift τ_m as $c_y = y/\tau_m$. Within the viscous sublayer $c_y/u_\tau \approx 1$ is found. For greater wall distances c_y increases.

Since τ_m^+ is not proportional to y^+ for $y^+ \gtrsim 5$, there are two possibilities to define a convection velocity using y^+ and τ_m^+. First, from the ratio of the wall distance, y^+, and

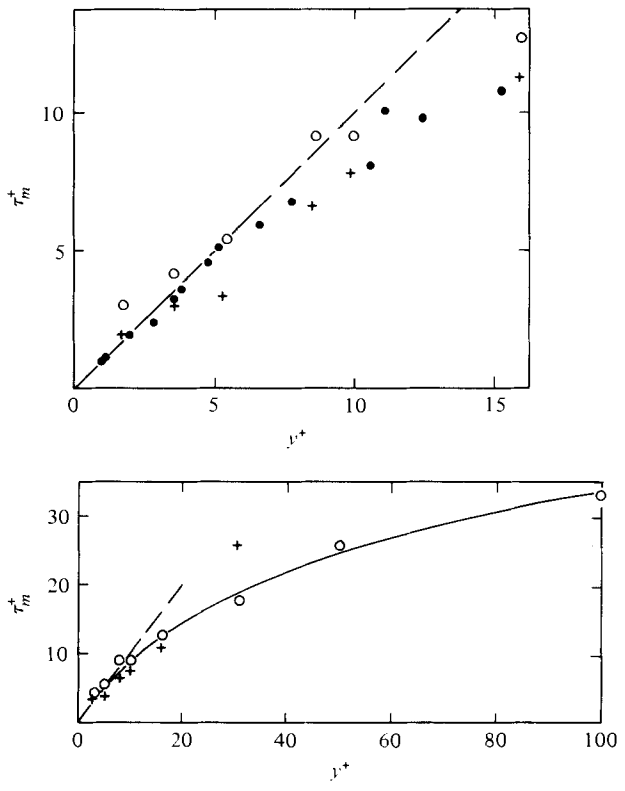

FIGURE 13. Time shifts for maximum correlation as a function of y^+.
○, R_{11}; +, R_{33}; ●, Eckelmann (1970).

the time shift, τ_m^+, one can obtain a velocity $c_y/u_\tau = y^+/\tau_m^+$. Secondly from the slope of the curve $\tau_m^+ = f(y^+)$, a velocity $c_y'/u_\tau = dy^+/d\tau_m^+$ can be derived. Within the viscous sublayer there is no difference between both velocities, hence $c_y = c_y'$. In figure 14, the convection velocities, c_y and c_y', for the perturbations of both the streamwise and spanwise fluctuations are shown as a function of the wall distance y^+. Within the experimental accuracy, the same velocities are obtained for both components.

The physical interpretation for the convection velocity normal to the wall will be postponed until the discussion. It should be pointed out, however, that this velocity is not related to a fluid motion toward the wall which cannot exist in the mean by continuity.

5. Space–time correlations of the streamwise and spanwise velocity fluctuations

Further correlation measurements of the streamwise and spanwise fluctuations, u and w, of the velocity were carried out using two V-probes at different x and y locations. The wall elements at the locations $x^+ = -108$, 0 and $+144$ were successively replaced by a wall plug on which a V-probe at a wall distance of $y^+ = 2{\cdot}3$ was mounted.

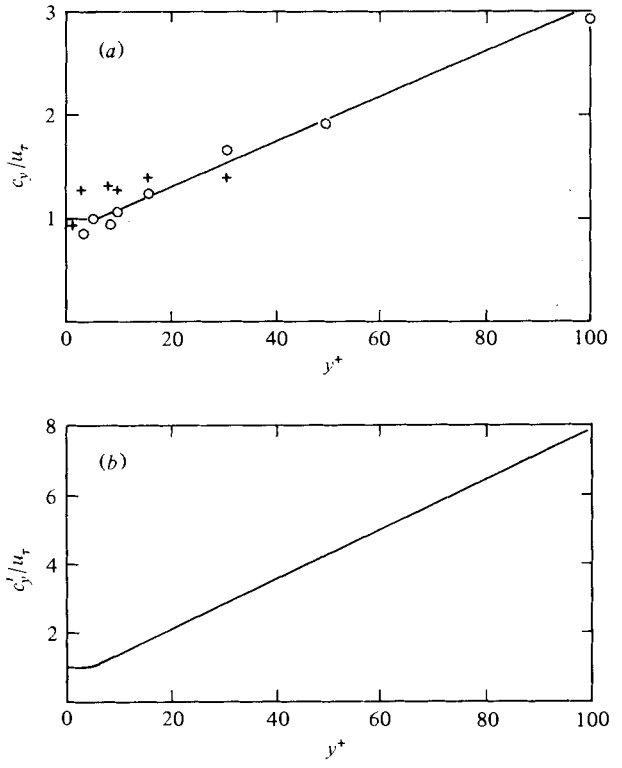

FIGURE 14. Convection velocities defined by $c_y = y/\tau_m$ in (*a*) and $c'_y = dy/d\tau_m$ in (*b*) as a function of y^+. ○, R_{11}; +, R_{33}.

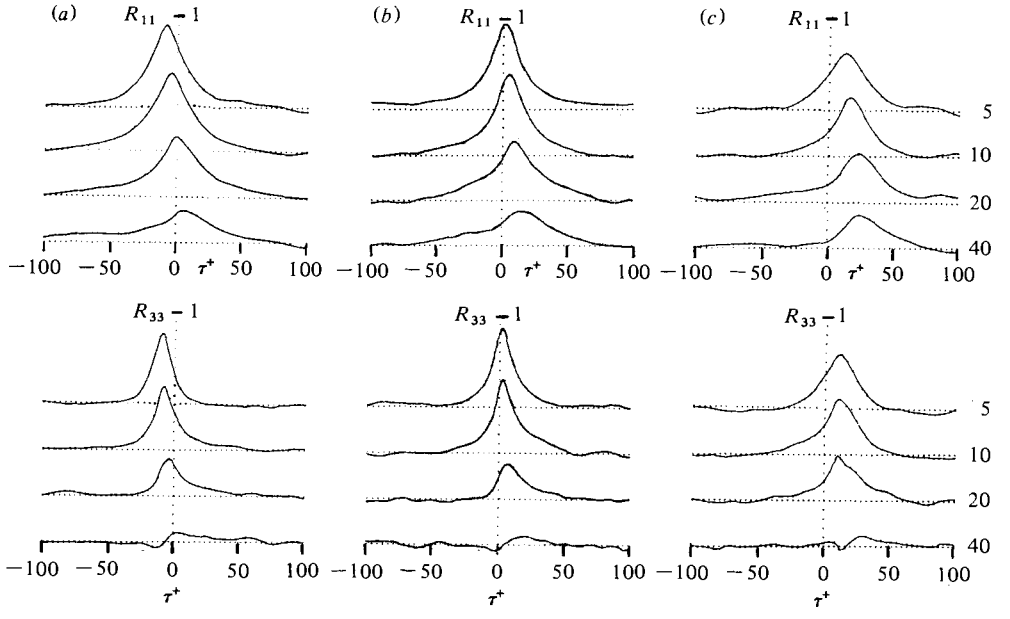

FIGURE 15. Space–time correlations of u and w for (*a*) $\Delta x^+ = -108$ and $\Delta z^+ = 0$, (*b*) $\Delta x^+ = \Delta z^+ = 0$ and (*c*) $\Delta x^+ = 144$ and $\Delta z^+ = 0$ as a function of y^+.

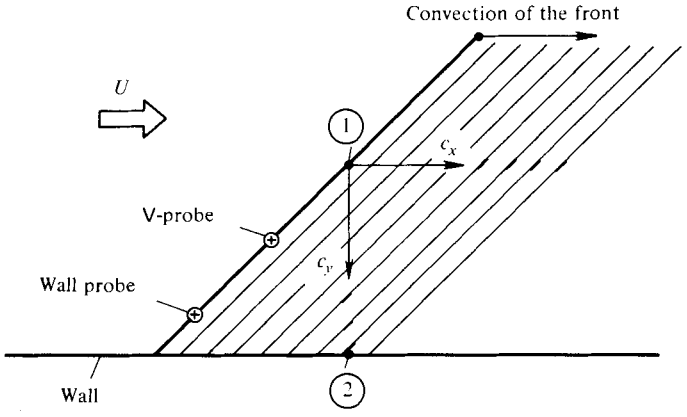

FIGURE 16. Sketch illustrating a front inclined to the wall which moves at a convection velocity c_x downstream. 1 and 2 are positions referred to in the text.

The movable V-probe was located at $x^+ = 0$ and $y^+ = 5$, 10, 20 and 40. In this way three different sets of correlation curves $R_{11}(\Delta x^+, y^+, \tau^+)$ and $R_{33}(\Delta x^+, y^+, \tau^+)$ were obtained and are shown in figure 15. The correlation functions $R_{11}(0, y^+, \tau^+)$ and $R_{33}(0, y^+, \tau^+)$ were obtained under similar conditions as those shown in figure 12 where, instead of the wall probe at $y^+ = 2{\cdot}3$, a wall element was used. The time shifts of the maxima obtained from figure 12 and from figure 15 for $\Delta x^+ = 0$ should only differ by the constant time τ_0 which is needed for the perturbations to travel from the location of the wall probe to the wall. A comparison of the times τ_1 obtained from figure 12 with the corresponding times τ_2 of figure 15 yielded that $\tau_1 > \tau_0 + \tau_2$ implying that the perturbations travel faster than expected from the location of the V-probe to the wall probe.

Based upon the various correlation measurements reported here, a model of the structure in the vicinity of the wall and adjacent wall region will be suggested in the next paragraph.

6. Discussion and conclusions

From the locations of the maxima of the correlation functions $R_{11}(\Delta x^+, \tau^+)$, $R_{33}(\Delta x^+, \tau^+)$ and $R_{11}(y^+, \tau^+)$, $R_{33}(y^+, \tau^+)$ (figures 5 and 12) delay times τ_m^+ have been obtained. These times together with the corresponding distances Δx^+ or y^+ were used to define two velocities c_x and c_y. The convection velocity c_y can easily be misinterpreted as a motion towards the wall which on the average does not exist. However, c_y does exist when a front is inclined to the wall and moving at a convection velocity c_x downstream as shown in figure 16. Clearly, c_y would be zero for a front perpendicular to the wall. A front can in actuality be any perturbation in velocity that occurs in a correlated manner in space. For example, if two probes were located as shown in figure 16 (i.e. the wall probe upstream of the V-probe) it is possible that both probes could simultaneously sense a perturbation. This was shown for the streamwise velocity component, u, in figure 15 for $\Delta x^+ = -108$ and $y^+ = 20$.

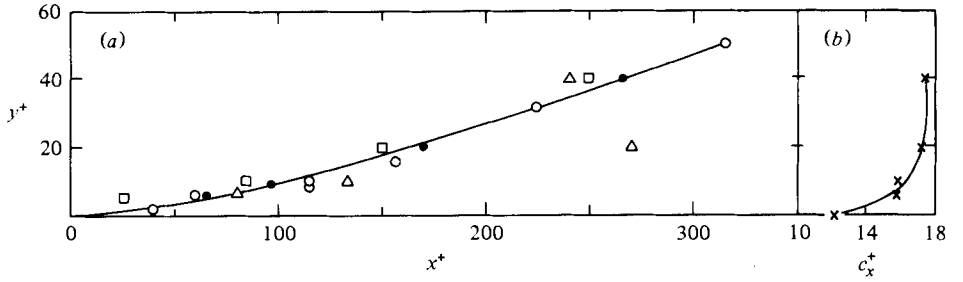

FIGURE 17. (a) Averaged front obtained from: ○, R_{11} ($\Delta x^+ = 0$, y^+, τ^+); ●, R_{11} ($\Delta x^+ = 0$, y^+, τ^+); □, R_{11} ($\Delta x^+ = -108$, y^+, τ^+); △, R_{11} ($\Delta x^+ = 144$, y^+, τ^+). (b) Convection velocity of the front $c_x^+ = c_x/u_\tau$ as a function of y^+.

An average front can be constructed from the data given in the previous paragraphs in the following way: Let the difference in the time between the front's arrival at positions 1 and 2 (figure 16) be τ_m, then, during this time the front has travelled along the wall the distance $x = \tau_m c_x$. By plotting the corresponding wall distances, y^+, versus the calculated x^+ values the average front shown in figure 17 is obtained. For the limiting case at the wall, where both convection velocities c_x and c_y have been measured, the angle between the front and the wall is $\varphi = \arctan(c_y/c_x) = 4{\cdot}7°$.

Points obtained from the V-probe wall probe measurements are also inserted in figure 17. For this case, the space–time correlations described in paragraph 5, showed that the front arrives at the wall probe earlier than estimated from the V-probe wall-element measurements. This means, that like c_y the convection velocity c_x also increases with increasing wall distance which leads to the picture that the slope of the front always decreases when travelling downstream. Using this conception, c_x was calculated for the various wall distances of figure 15 and is shown as a function of the wall distance, y^+, in figure 17; at the wall c_x was measured as described in paragraph 3.

Using the convection velocities, $c_x(y^+)$, and the corresponding time shifts, τ_m, obtained from figure 15, the resulting distances x^+ for the various wall distances y^+ were calculated and inserted into figure 17. For the case that the wall probe was located downstream or upstream of the V-probe, the constant distance $\Delta x^+ = 144$ or $\Delta x^+ = -108$ respectively, was added to the calculated distance x^+. Then within a relatively small range of scatter all V-probe wall-probe measurements collapse on the same curve with those of the V-probe wall-element combination.

The fronts in the wall region are very distinct and frequently occurring because of the relatively high correlations obtained. As an example the maximum correlation is nearly 40% for R_{11} ($\Delta x^+ = 144$, $y^+ = 40$). In this case the front travels from the V-probe at $x^+ = 0$ and $y^+ = 40$ over a distance of about one channel width before the second probe at $x^+ = 144$ and $y^+ = 2{\cdot}3$ is reached. The spanwise velocity fluctuations do not show as pronounced fronts as do the streamwise fluctuations. In addition, the correlation functions R_{33} show, for wall distances $y^+ > 5$, an increasing skewness and, for $y^+ \geqslant 40$, a totally different shape (compare figures 12 and 15).

Kovasznay, Kibens & Blackwelder (1970) discussed three types of correlation curves and the time functions which produce them. One type is a symmetric correlation function which in this investigation is always observed when the streamwise fluctuations are correlated. Another type, an antisymmetric correlation function, is

obtained in the present work for the correlations of the spanwise fluctuation for $y^+ \gtrsim 40$. The skewed correlation functions at $5 \lesssim y^+ \lesssim 40$ indicate the change from the symmetric to the antisymmetric function (compare figures 12 and 15). The antisymmetric correlation function is produced by a symmetric and an antisymmetric time function. Such time functions exist if it is supposed that the fronts originate from inclined streamwise vortices. A probe positioned at a wall distance of $y^+ = 40$ senses the fluid flowing in the same spanwise direction as the wall probe at $y^+ = 2{\cdot}3$ as long as the vortex centre is above $y^+ = 40$. When the vortex has travelled further downstream and the vortex centre is below $y^+ = 40$, then both probes sense the fluid flowing in opposite spanwise directions. Since the flow direction at the wall probe is not changing, whereas it does at the V-probe, an antisymmetric correlation function due to Kovasznay *et al.* is expected and observed here (figure 15). If the V-probe is positioned at $y^+ \lesssim 10$ both probes are always below the vortex centre which leads to a symmetric correlation function. From the change of the correlation functions' shape between $10 < y^+ < 20$ (figure 15) the average minimum distance of the vortex centre can be estimated to $y^+ \approx 30$.

In accordance with the measurements of Blackwelder & Eckelmann (1979) from figures 9 and 10 follows that these vortices appear as pairs with opposite rotation and with an average spanwise separation of their centres of about $\Delta z^+ \approx 50$. The length of these vortices can be estimated to $\Delta x^+ \approx 1200$ (figure 7). As the vortices are convected downstream, the angle of inclination of the plan of their rotation is decreasing. These vortices pump fluid away from the wall forming low speed streaks and toward the wall forming high speed streaks. The spanwise distance of the low speed streaks has been measured by Kim *et al.* (1971) and Oldaker & Tiederman (1977) using visualization techniques and by Gupta *et al.* (1971) using hot-wire probes. They all observed an average streak spacing of $\Delta z^+ \approx 100$, which is consistent with the conclusions and measurements (figure 9) above.

Pairs of counter-rotating streamwise vortices in the wall region were also observed by Bakewell & Lumley (1967) and they found that the mean distance of the vortex centres from the wall is $y^+ \approx 35$. Lee *et al.* (1974) also concluded from correlation measurements of the streamwise and spanwise velocity gradients at the wall that counter-rotating streamwise vortices with a mean spacing of $\Delta z^+ \approx 50$ exist.

A comparison of the correlation functions $R_{11}(y^+, \tau)$ with $R_{33}(y^+, \tau)$ shown in figure 12 indicates that the correlations of the spanwise component decrease faster with increasing wall distance than the correlation of the streamwise component. A possible explanation for this could be that the sweep motion observed by Corino & Brodkey (1969) and the high speed fronts of Nychas *et al.* (1973) and Eckelmann *et al.* (1977) contribute more to the correlation R_{11} than to R_{33}. The lifted up low speed streaks of Kim *et al.* (1971) would also be in accordance with the front model.

In a turbulent boundary layer Brown & Thomas (1977) used an array of hot-wires and wall-elements to make correlation measurements. From the correlation between the wall gradient and the velocity at various wall distances, they found structures with an oblique angle to the free stream direction. Also in a turbulent boundary layer Chen & Blackwelder (1978) using temperature as a passive contaminant found a sharp internal temperature front inclined to the wall. The present work was made in a turbulent channel flow. Both turbulent boundary layer and channel flow show in the wall region these distinct fronts.

The authors wish to thank Prof. Dr E.-A. Müller for his interest in this work, Messrs. K.-H. Christmann, K.-H. Nörtemann and H. J. Schäfer for their technical aid and Mr P. Habermann for his advice with the computer. We should like to thank Profs. R. F. Blackwelder, R. S. Brodkey and J. M. Wallace for various discussions and their help with the translation. Mrs Ch. Köneke typed the manuscript and Mrs L. Wahle made the drawings.

REFERENCES

BAKEWELL, H. P. & LUMLEY, J. L. 1967 *Phys. Fluids* **10**, 1880.

BLACKWELDER, R. F. & ECKELMANN, H. 1978 *Structure and Mechanisms of Turbulence. I* (ed. H. Fiedler), Lecture notes in physics, vol. 75, p. 190. Springer.

BLACKWELDER, R. F. & ECKELMANN, H. 1979 *J. Fluid Mech.* **94**, 577.

BLAKE, W. K. 1970 *J. Fluid Mech.* **44**, 637.

BROWN, G. L. & THOMAS, A. S. W. 1977 *Phys. Fluid Suppl.* **20**, S 243.

BULL, M. K. 1967 *J. Fluid Mech.* **28**, 719.

CHEN, C.-H. P. & BLACKWELDER, R. F. 1978 *J. Fluid Mech.* **89**, 1.

CORINO, E. R. & BRODKEY, R. S. 1969 *J. Fluid Mech.* **37**, 1.

CORRSIN, S. 1957 Sym. on Naval Hydrodyn. Publ. 515 NAS-NRC 373.

ECKELMANN, H. 1970 *Mitt. MPI Strömungsforschung and AVA Göttingen* no. 48.

ECKELMANN, H. 1974 *J. Fluid Mech.* **65**, 439.

ECKELMANN, H., NYCHAS, S. G., BRODKEY, R. S. & WALLACE, J. M. 1977 *Phys. Fluid Suppl.* **20**, S 225.

EMMERLING, R. 1973 *Mitt. MPI Strömungsforschung and AVA Göttingen* no. 56.

EMMERLING, R., MEIER, G. E. A. & DINKELACKER, A. 1974 *AGARD Conf. Proc.* no. 131 *on Noise Mechanisms*, pp. 24–1 – 24–12.

GUPTA, A. K., LAUFER, J. & KAPLAN, R. E. 1971 *J. Fluid Mech.* **50**, 493.

KIM, H. T., KLINE, S. J. & REYNOLDS, W. C. 1971 *J. Fluid Mech.* **50**, 133.

KLINE, S. J., REYNOLDS, W. C., SCHRAUB, F. A. & RUNSTADLER, P. W. 1967 *J. Fluid Mech.* **30**, 741.

KOVASZNAY, L. S. G., KIBENS, V. & BLACKWELDER, R. F. 1970 *J. Fluid Mech.* **41**, 283.

KREPLIN, H.-P. 1976 *Mitt. MPI Strömungsforschung and AVA Göttingen*, no. 63.

LAUFER, J. 1975 *Ann. Rev. Fluid Mech.* **2**, 95.

LEE, M. K., ECKELMAN, L. D. & HANRATTY, T. J. 1974 *J. Fluid Mech.* **66**, 17.

NYCHAS, S. G., HERSHEY, H. C. & BRODKEY, R. S. 1973 *J. Fluid Mech.* **61**, 513.

OFFEN, G. R. & KLINE, S. J. 1974 *J. Fluid Mech.* **62**, 223.

OLDAKER, D. K. & TIEDERMAN, W. G. 1977 *Phys. Fluid Suppl.* **20**, S 133.

SIMPSON, R. L. 1976 *MPI Strömungsforschung Göttingen, Rep.* no. 118/1976.

SIRKAR, K. K. & HANRATTY, T. J. 1970 *J. Fluid Mech.* **44**, 605.

WALLACE, J. M., BRODKEY, R. S. & ECKELMANN, H. 1977 *J. Fluid Mech.* **83**, 673.

WALLACE, J. M., ECKELMANN, H. & BRODKEY, R. S. 1972 *J. Fluid Mech.* **54**, 39.

WILLMARTH, W. W. 1975 *Adv. Appl. Mech.* **15**, 159.

WILLMARTH, W. W. & WOOLDRIDGE, C. E. 1962 *J. Fluid Mech.* **14**, 187.